Strengthening tropical cyclones are associated with more frequent hazardous material pipeline failures in the Eastern US

M. Smith[1] and E. Carter[1,*]

[1] *Civil and Environmental Engineering, Syracuse University, Syracuse, NY 13244, USA*
[*] *corresponding author, ekcarter@syr.edu*

May 14, 2025

Abstract

Over 30,000 hazardous material pipeline (HMP) failures have caused nearly $11 billion in damages since 1970. Tropical cyclones, which cause more infrastructure damage than all other forms of natural disasters combined, are under-reported causes of HMP failures, largely due to historic policy around pipeline failure reporting. This study defines tropical cyclone-associated HMP failure frequency based on spatiotemporal concomitance while detrending for background HMP failure rates. The relationship between the likelihood and frequency of HMP failures and tropical cyclone intensity is characterized. Since 1975, the annual frequency of tropical cyclone-associated pipeline failures has increased by an order of magnitude. Storm intensity is significantly related to the frequency of HMP failures, explaining 32% of spatial variability and 38% of inter-annual variability in local storm-level pipeline failure frequency. Since 1970, the average annual maximum tropical cyclone intersecting with HMP infrastructure has increased from a Category 3 to a Category 4 storm on the Saffir-Simpson hurricane scale. Assuming near-term conservation of historical meteorological trends, 200-500% increases in the number of pipeline failures occurring during the annual average maximum tropical cyclone are projected across the Eastern US by 2050. Implications of accurate natural hazards-related cause attribution on HMP failure incident reports are discussed.

Introduction

The United States' onshore hazardous material pipeline (HMP) network, spanning over 3.3 million miles, is a critical component of the nation's energy infrastructure. The majority of petroleum products used in the United States are transported through the HMP network. National dependence on HMPs has driven a nearly 14% expansion of pipeline in the past eight years ([1]) with an almost 30 million barrels per day increase in HMP transport projected by 2040 ([2]). Despite the benefits of HMP infrastructure, HMP infrastructure failures, which cause unintended discharge of petroleum products into the environment, are associated with devastating economic, environmental, and social costs ([3, 4]). Over 30,000 HMP failures have been reported in the United States since 1970. Between 2005-2023, reported HMP failures were associated with 274 fatalities, 1,120 injuries, and nearly $11 billion in damages ([5]). Between 28-95% of the total costs of pipeline failures are associated with environmental damage and remediation ([6, 7]), yet even with the large price tag, about 85% of products released remain unrecovered after remediation ([7, 8]), leading to long-lasting ecological and public health impacts.

In 1968, the Pipeline Safety Act mandated and outlined the requirements for reporting hazardous material pipeline (HMP) failures ([5, 9, 10]). This regulation requires pipeline operators to report HMP failures within 30 days of occurrence, providing accident-specific details such as location, facilities involved, operations, personnel conduct, and the cause of the incident. When reporting HMP failure cause, pipeline operators have historically selected a single cause from pre-defined categories, including corrosion, excavation damage, external forces, material or weld failures, equipment malfunctions, and incorrect operation. "Natural forces" was added as a causal category on HMP incidence reporting forms in 2002 (Text S1). In reality, HMP failures frequently result from the interaction of multiple contributing factors (for example natural force failures are more likely when there is underlying corrosion). Single-category cause attribution in mandated reporting therefore limits analysis of complex or interacting drivers of HMP failures ([11–13]).

Though estimates vary widely, meteorological events, specifically tropical storms and hurricanes (tropical cyclones, TCs), are reported to contribute significantly to total damages associated with natural-hazard triggered pipeline accidents in the United States ([14]), and have been estimated to be the cause of up to 86% of all natural-hazard mediated pipeline failures worldwide ([12]). While the true magnitude of natural-hazard-associated pipeline failures in the United States is difficult to estimate due to reporting bias ([15]), TCs are broadly understood to be an important, and under-characterized, driver of HMP failures ([12, 15]).

As average ocean temperatures across the Atlantic Basin continue to increase due to climate change ([16–18]), TCs, which are fueled by warm ocean temperatures, have increased in intensity ([19–21]). Previous research shows that the most damaging tropical cyclones—those categorized as three or higher—are responsible for approximately 85% of the total TC damages, even though they constitute 24% of landfalling storms ([22]). These extreme events are particularly challenging to simulate accurately in gridded climate models (e.g. [23]), leading to inconclusive findings in numerical studies on how anthropogenic climate change will impact the most powerful TCs. However, historical data analysis indicates a significant increase in the occurrence of high-intensity storms in particular as a result of sea surface temperature increases (Text S6, [19, 20, 24]).

Regulatory bodies across the world target HMP design standards on building network resilience to natural disasters, such as earthquakes in California ([25]) and tsunamis in Japan ([26]). TC storm tracks impact 19 US states, overlapping with some of the densest HMP infrastructure in North America (Fig 1a, [5]). TCs can stress pipeline systems through a variety of mechanisms, including but not limited to mechanical stress from high wind speeds; intense precipitation and related impacts including compound flooding; shifting and settling of rapidly saturated soils; erosion, accretion, and landslides; storm surges and related coastal impacts; and intensified tornado activity inland ([27–29]). Some of these stresses are acute, and can logically be associated with pipeline failure at low latency. For example, TC-associated tornado damage to an above-ground transmission pipeline is easily attributable to an individual storm event ([10, 30]). Many of these stresses are cumulative and can result in a decreased overall lifetime of the pipe system. For instance, a pipeline network subject to frequent bouts of wetting and drying due to TC-related precipitation in regions with high shrink-swell potential could undergo significant mechanical stress ([31, 32]); and pipelines impacted by saline storm surges coastally could experience more rapid rates of corrosion over time ([33, 34]). While impacts of high wind speeds and intense rainfall are universal, TCs interact with local soils, land cover, topography, and microclimate to generate different impacts on infrastructure in different regions of the United States. Coastal regions (Texas Coast, Mississippi Delta, Southeast Coast) will experience effects of storm surges ([35, 36]); flat regions (High Plains, Southeast Coast, Midwest) may see tornado activity [35, 37]); hilly regions (Northeast) may see compounding flooding, including coastal, riverine, and flash flooding and landslides ([38, 39]); and the High Plains, Texas, and Mississippi Delta region will likely be additionally impacted by high shrink-swell potential of local soils saturated with intense rain over large geographic reaches ([40, 41]).

To inform dialogue on engineering standards for HMP failure reporting, design, and maintenance in hurricane-prone regions in the 21st century, the objective of this study is to quantify associations between trends in HMP failure frequencies and observed increases in TC intensity (TCI, the first principal component of maximum sustained near-surface windspeed and minimum se-level pressure) associated with climate change. As there are no historical records of TC associated storm failures available through the PHMSA, we identify HMP failures that have occurred after exposure to TCs, while detrending for background regional failure rates unassociated with storms. Utilizing a simple modeling framework that can control for, and quantify the relative importance of, unparameterized spatiotemporal drivers of HMP failure, we estimate the extent to which increases in TCI observed in the last 50 years are associated with increased TC-related failure frequencies (Text S2 and S3, Figure 1b) during the same time period. We confirm conclusions from the literature [12–14, 35] suggesting that the average annual maximum storm intersecting with HMP infrastructure has increased from a Category 3 storm on the Saffir-Simpson Hurricane Scale in 1970 to a Category 4 in 2010. In the absence of robust numerical models, we resort to extrapolating from this trend to assume a linear increase in TCI associated with increasing sea surface temperatures in the subtropical Atlantic up until 2050, when regional SSTs are projected to reach the 26.5°C threshold after which thermodynamic intensification of TCs is expected to "saturate" and break from linear trends ([42]). Assuming near-term continuation of observed linear trends implies that the average annual maximum storm intersecting with HMP infrastructure will be a Category 5 by 2050 (Text S6). Our models suggest that HMP failures are both more significantly more likely, and exponential more frequent, as storm intensity increases. These results underscore the significance of meaningful design interventions to stabilize HMPs in TC regions, and suggest that TCs need to be attributable as contributing causes of HMP failure on incidence reporting forms for accurate attribution.

Results

Pipeline Failure Attribution Analysis

Between 1986 and 2022, pipeline failures in the PHMSA dataset were categorized as resulting from natural forces (4.3%, or 275 failures), human error (14.9%, or 943 failures), and external forces (80.8%, or 5,124 failures). The first recorded pipeline failure attributed to "natural forces" appeared in 2002 when the category was introduced, with no significant positive or negative trends in the frequency of this attribution observed since then (Figure S1). In contrast, significant ($p < 0.01$) positive trends were noted in the annual frequency of failures attributed to human error (an increase of 1.33 failures per year) and external forces (an increase of 1.45 failures per year) over the same period (Figure S1). Spatiotemporal characteristics of pipeline network (including but not limited to the total length of pipeline in a region, the rate at which regional pipeline networks are expanding, and aging pipe) will influence current and future regional baseline and HMP failure frequencies. To account for regional differences in HMP infrastructure (such as pipeline density), as well as regional differences in TC dynamics, we divided the study area into six spatial subregions using K-means clustering on latitude and longitude (Figure 1a, Text S1). In all models, we set random intercepts to these location groups, as well as to individual years, to control for spatiotemporal non-independence in the data that could bias our estimators.

Although PHMSA reports attribute a relatively low percentage of pipeline failures to "natural forces," our analysis found that 32.5% of HMP failures in the TC intersecting region occur within 60 days of TC exposure (Figure S2),

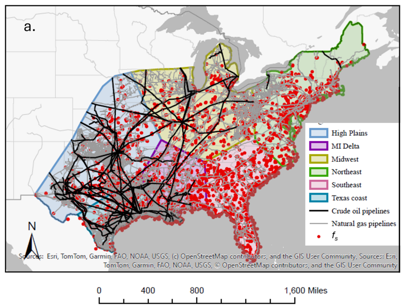

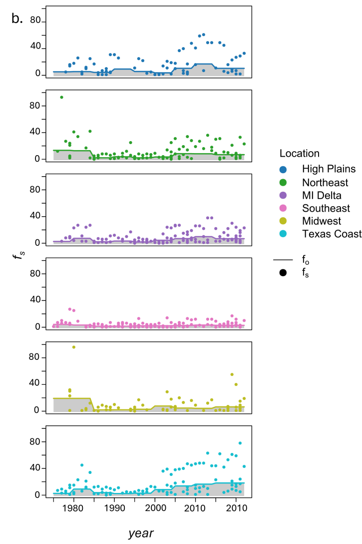

c.

region	TC max windspeed (knots)	Crude oil: pipeline length (m)	Natural gas: pipeline length (m)	Total TC-related failures (fs')
Midwest	50	9.33.E+06	4.84.E+07	153
Southeast	145	NA	1.40.E+07	154
High Plains	70	1.99.E+07	8.15.E+07	191
Northeast	100	4.33.E+05	2.73.E+07	263
MI Delta	140	5.86.E+06	4.57.E+07	322
Texas Coast	115	1.06.E+07	6.14.E+07	498

Figure 1: a. Six spatial sub-regions where HMP infrastructure (major crude oil and natural gas transmission pipelines, [43]) intersect with tropical cyclone storm tracks (TCs) in the continental United States. b. Time series of f_s (points) and f_o (lines) by spatial region. Points above the grey polygon represent storm-related HMP failures, or f'_s. c. For each spatial sub-region, table indicates total 1970-2022 f'_s, maximum TC windspeed, length of crude oil pipeline, and length of natural gas pipeline. Here "MI Delta" refers to "Mississippi Delta"

which serves as our temporal cutoff point for a TC-associated HMP failure (Text S1). Over the study period, we observed a significant positive linear trend in the annual frequency of failures occurring within 60 days of TC exposure (the regional TC-associated failure frequency, or f_s, Eq. 1). Drawing from this trend, in 1975, the annual mean f_s in the Eastern US was 4 TC associated failures; by 2020, this number had risen to 50 failures per year (Figure S3). As trends in f_s will be associated with both failures related to TC, as well background failures that would have occurred regardless of TC exposure, we also quantify the local, time-dependent background failure frequency (f_o , Eq. 2, Figure 1b), and define the TC-related failure frequency (f'_s), as f_s minus the time-dependent regional 60-day background failure frequency (f_o, Eq. 3, Figure 1b).

The highest total number of TC-related HMP failures (f'_s) were observed on the Texas coast, followed by the Mississippi Delta and Northeast regions; where high-magnitude TCs (indicated by wind speed) intersect with dense crude and natural gas pipelines (Figure 1c). More frequent f'_s are observed in the second half of the study period relative to the first in the Mississippi Delta and Texas coast, indicative of a trend in these regions (Figure 1b). Higher pipeline failure per unit length of crude oil pipeline is observed in the Northeast than other regions (Figure 1c). High magnitude f_s' is observed in High Plains, despite lower maximum TC wind speed (Figure 1b,c). The Southeast returns few f_s' relative to high TC wind speeds, likely because of a lack of crude oil pipeline infrastructure in the region, and frequent number of storms (Figure 1c).

To evaluate whether more the intensity of TCs modifies the likelihood of at least one HMP failure, we utilized a mixed-effects logistic regression model predicting the likelihood of at least one f_s' per region for a storm, with random intercepts on region and year. TC intensity (or TCI, calculated as the first principal component of the maximum sustained near-surface windspeed and minimum sea-level pressure of all storm HURDAT2 points intersecting with with a spatial subregion) is a statistically significant predictor of one or more HMP failures for a given region (at α=0.05), with the likelihood of one or more failure increasing by 59% for a standard deviation increase in TCI (Text S7, Figure S7a). This indicates that with a TCI of zero, approximately equal to the interface between a tropical cyclone and Category 1 hurricane on the Saffir-Simpson hurricane scale (Fig 3c), the probability of at least on HMP failure is about 20%. According to this model, the probability of at least on failure increases to 31% for a Category 2 storm, 38% ffor a Category 3 storm, 49% for a Category 4 storm, and 64% for a Category 5 storm. TCI explains minimal inter-annual variance (v) in the likelihood of one or more HMP failure (0.2%), but explains 21.8% of the regional variance (u) (Figure S7b,c), suggesting that variable TCI explains about 22% of the spatial variability in the likelihood of at least one HMP failure. The likelihood of TC-related HMP failure is higher in the Mississippi Delta, Texas Coast, and Northeast region (Figure S7b).

Nested mixed-effects Poisson regression models characterize how TCI modifies the frequency of pipeline failures, while controlling for spatiotemporal non-independence in the data with random intercepts on year and location. TCI is a statistically significant (at $\alpha < 0.001$) predictor increased frequency of pipeline failures f_s', with an incidence rate ratio of 1.54 averaged across the region. If we look at how this translates to f_s' in Texas, for example, this suggests that the after failure frequency for a Category 1 storm is about 5. This increases to 9 f_s' for a Category 2 storm; 15 f_s' for a Category 3 storm; 28 f_s' for a Category 4 storm; and 63 f_s' for a Category 5 storm. Adding TCI explains 24% of variance in location (u) and 34% of residual variance in year (v) (Figure 2a, Text S8). In the null model, inter-annual variance in f_s' (v) was 141% greater than regional variance (u) implying that inter-annual variability in f_s' for a given location is greater than regional variability in f_s' within a given year.

In the null model, u_j and v_k indicate anomalies in f_s' from year to year and location to location. Shifts in u_j and v_k between a null model (no fixed effects) and the full model (containing TCI as a fixed effect) indicate inter-regional and inter-annual variability in how f_s' responds to TCI (Figure 2b,c). In the null model, the highest u_j, corresponding to the highest regional average regional f_s', is observed along the Texas Coast, followed by the Mississippi Delta and the High Plains. The lowest u_j, corresponding the lowest f_s' for a region, are observed in the Southeast and in the Midwest. Negative shifts in u_j in the Texas Coast and Mississippi Delta with TCI parameterized suggests that a substantial portion of the high f_s' observed in this region is explained by increased TCI. A positive shift in u_j in the High Plains suggests that the global coefficient on TCI may lead to an underestimation of TC-related pipeline failures (f_s') for low-intensity TCs, which most frequently present in the region (Fig 1b). A positive shift in the negative u_j in the Midwest suggests that lower (f_s') in the region is partially explained explained by lower TCI in the Midwest, relative to other regions (Figure 2b).

The random intercept on year (v_k) in the null model likewise indicates the relative anomaly in (f_s') for a given year. Evaluating the color scale, we observe 14 out of 20 of the latest years (2002-2022) with a positive v_k, and only 6 out of the 20 latest years with a negative v_k, indicating a trend towards increasing f_s' over time. Reduction in the absolute value of v_k between null and full models highlight years when TCI explains anomalies in f_s'. Strong negative shifts are observed in positive intercepts in 2014, 2005, 2017, 1992, and 2012, suggesting that TCI explained more of the anomalously high (f_s') in these years (Figure 2c, Text S9).

Trends in Tropical Cyclone Dynamics

Between 1977 and 2022, 579 out of 729 tropical cyclones (TCs) in the NOAA HURDAT2 Atlantic Basin database intersected with HMP infrastructure (HMP intersecting TC) in the Central and Eastern United States. For each year, the strongest HMP intersecting TC is identified. There is evidence that the strongest annual HMP interscted TC is getting stronger over time. Since 1975, a significant positive linear trend in components of TCI (maximum sustained near-surface windspeed and minimum sea-level pressure) are observed. That the annual maximum sustained HMP-intersecting TC windspeed has been increasing by about 0.6 knots per year since 1975, corresponding to a 27.6 knot increase over the 46 study period. To put this number in perspective, the difference in windspeed between a Category 2 storm and a Category 4 storm on the Saffir Simpson hurricane scale is 18 knots. Similarly, we observe a significant negative linear trend in annual minimum TC pressure (where decreasing pressures indicate increasing storm intensity) by -0.7 mBar per year (Fig 4a-b). This result is unsuprising given that maximum windspeed and minimum pressure are highly collinear.

Drawing from these trends, the annual maximum wind speed and minimum pressure of an HMP intersecting TC in 1970 was approximately 107 knots and 954 mBar, respectively; corresponding to a Category 3 hurricane on the Saffir-Simpson Hurricane Scale. In 2010, the annual maximum wind speed and minimum pressure of an HMP intersecting TC were 130 knots and 928 mBar, respectively; corresponding to a Category 4 hurricane. Projecting this trend to 2050 produces an estimated annual maximum wind speed and minimum pressure of 154 knots and 902 mBar, respectively; corresponding to a Category 5 storm (Figure 3c, yellow bars). 2050 projections are presented for illustrative purposes only. Linear interpolation of hurricane strength based on time, when we assume that the physical driver of this increase in strength is increasa.

Predictors	Null model *Incidence Rate Ratios*	TCI *Incidence Rate Ratios*
Intercept	0.30 **	0.35 **
TCI		1.54 ***
Random Effects		
σ^2	1.47	1.78
τ_{00}	1.52 $_{\text{yr}}$	0.95 $_{\text{yr}}$
	0.63 $_{\text{locGrp}}$	0.43 $_{\text{locGrp}}$
N	46 $_{\text{yr}}$	46 $_{\text{yr}}$
	6 $_{\text{locGrp}}$	6 $_{\text{locGrp}}$
Observations	350	350
AIC	1042.293	915.009
log-Likelihood	-518.146	-451.504

* *p<0.05* ** *p<0.01* *** *p<0.001*

b.

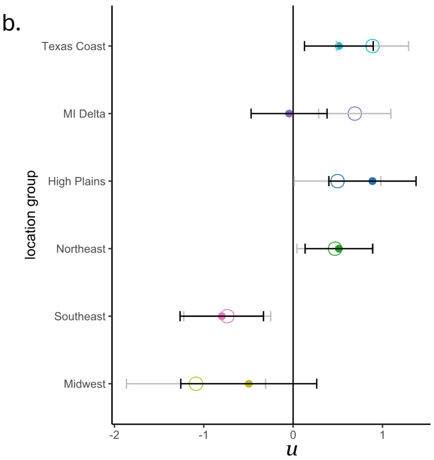

c.

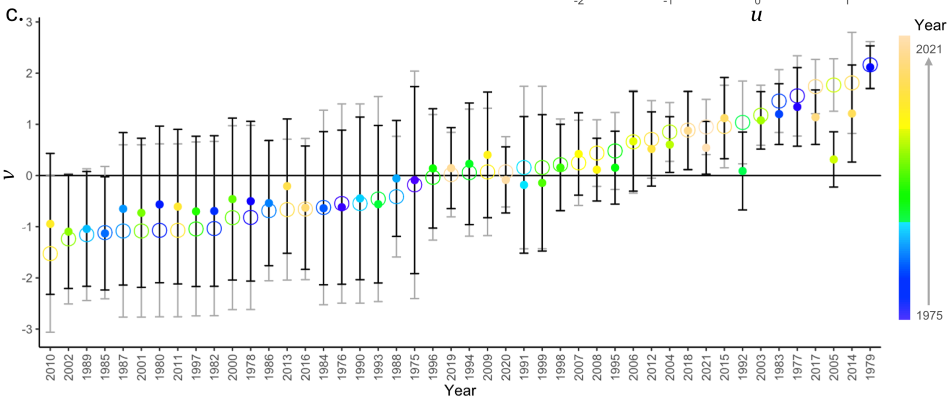

Figure 2: a) Mixed-effects Poisson model parameters and statistics for null (no fixed effects) and full (TCI as a fixed effect) models, b) caterpillar plot of random intercept (points) on location for null (open circles) and full (closed circles) models, with error bar representing 95% confidence interval; color scale indicating location group c) as in b but for random intercept on year, with color scale indicating advancing year. Here, "MI Delta" refers to "Mississippi Delta".

ing sea surface temperatures under climate change, rests on physically flawed assumptions (Text S6) . Incidentally, significant southeastern shifts in origin coordinates of the annual maximum TC intersecting with HMP infrastructure (corresponding to a 0.15 degrees/year southerly and 0.41 degree/year easterly shift) were also observed, consistent with the literature (e.g [44], Figure S9). Projected maximum annual TCs represent the highest-magnitude storm that could be expected to impact the Gulf Coast regions (Texas coast, Mississippi Delta, and Southeast) on an annual basis, and corresponding f_s' projections for the annual maximum TC are indicated on Figure 3c.

Projecting from local trends in TCI, the Mississippi Delta and Texas Gulf Coast regions are projected to see an over 5-fold increase in the frequency HMP failure associated with the local annual maximum TC (f_s' associated with the TC with the highest windspeed per location group); the High Plains is projected to see a four-fold increase in f_s' with the annual maximum TC by 2050, the Northeast a nearly 3 fold increase in f_s' with the annual maximum TC , and the Southeast and Northeast are expected to see a doubling f_s' per annual maximum TC by 2050 (Figure 3d). These projections suggests a 200-500% increase in HMP failure frequency, independent of drivers of background HMP failures such as increased pipe age or length (f_o), associated with the local annual maximum TC across the Eastern US in 2050.

Discussion

TC-related HMP failure (f_s') are more likely, and exponentially more frequent, for stronger hurricanes. The greatest TCI related increases in f_s' are observed along the Texas and Mississippi coasts, regions with dense crude oil pipeline infrastructure, high shrink-swell potential of local soils, and exposure to coastal storm surges and high-intensity TCs ([6, 15]). Increased frequency of f_s' associated with even small shifts in TCI is observed in the High Plains, where only low-intensity storms have occurred, indicating sensitivity of High Plains HMP infrastructure to intensity- invariant impacts of TCs, such as associated tornado activity and interactions between intense precipitation and high shrink-swell potential of local soils, which can put significant mechanical stress on underground pipeline networks ([31, 32, 41]). Lack of crude oil pipeline infrastructure equates to a significant reduction in overall HMP pipeline failure associated with extreme events on the Southeast coast, despite exposure to frequent, intense TCs (Figure 1, 3c).

Significant linear trends are observed in the strength of the annual maximum TCI during the study period indicate that the annual maximum TC intersecting with HMP infrastructure has increased from a Category 3 to a Category 4 between 1970-2010. Linear trends in TCI noted here are both notable in terms of their magnitude and in terms of their consistency with previous research ([45–48]). In using this observed trend to predict the strength of the future annual maximum storms, we make important assumptions about the physical drivers of TCs. The first assumption is that hurricanes are powered by temperature

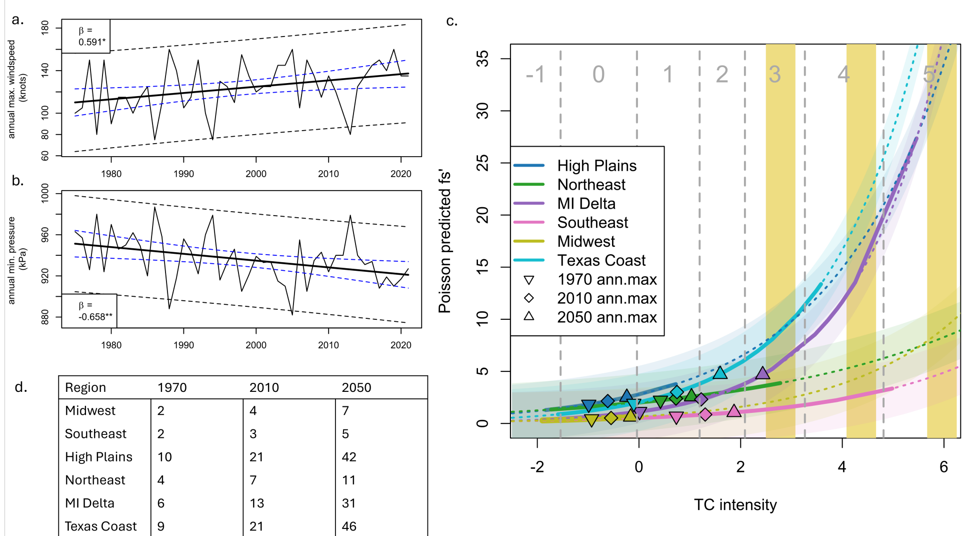

Region	1970	2010	2050
Midwest	2	4	7
Southeast	2	3	5
High Plains	10	21	42
Northeast	4	7	11
MI Delta	6	13	31
Texas Coast	9	21	46

Figure 3: Linear trends in 1975-2022 annual maximum HMP intersecting a) maximum sustained near-surface windspeed and b) minimum sea-level pressure. c) Poisson projected f_s' (Eq 3) by region (color), with range of observed historical regional TCI indicated by solid lines and out-of-sample projections indicated with dashed lines. Inverted triangle, diamond, and triangle symbols correspond to the annual maximum regional TCI projected from linear trends for 1970, 2010, and 2050 (Fig S6). Yellow bars represented maximum projected HMP intersecting TCI for 1970 (left), 2010 (center), and 2050 (right); extrapolated from linear trends observed 1975-2022 (Figure 2a,b). Dashed vertical gray lines represent storm classification thresholds on the Saffir-Simpson Hurricane Scale, with corresponding storm classification indicated as text along top of figure. Table 3d contains projected f_s' by region for 1970, 2010, and 2050 maximum annual HMP infrastructure intersecting TCI (yellow bars). Here, "MI Delta" refers to "Mississippi Delta".

differences between the warm sea surface and the cold upper atmosphere. There is scientific consensus on this principle (e.g. [49]). The second assumption is that sea surface temperatures (SSTs) in the subtropical Atlantic, where Atlantic TCs originate, are increasing because of anthropogenic climate change. There is emerging scientific consensus backing this assumption, with multiple studies documenting robust trends in SSTs over time ([50–52]), in line with what would be expected from physics-based coupled earth systems models ([53, 54]). The third assumption is that the historical relationship between SST and hurricane strength will remain non-stationary over time. There is strong physical evidence countering the realism of this assumption. First, there are thermodynamic limits to SST-associated TC strength increases over time: climate change is driving both increases in SST and increases in temperatures in the upper atmosphere, reducing the vertical temperature contrast that drives TC formation ([42, 49]). In numerical models, once subtropical Atlantic SSTs get above a certain threshold ($\tilde{2}6.5$°C), a "saturation" of this TC strengthening effect is noted, and SST warming yields smaller increases in TC strength ([42]). This is both due to energy limitations to atmospheric vapor storage, and because climate change is also modifying other atmospheric drivers and constraints of hurricane formation, such as wind shear, humidity levels, and vertical stability; all which impact TC formation and propagation in complex ways ([55]). Finally, not all of the energy from increasing SSTs will be dissipated as increased windspeeds in TCs. Increased energy available for TCs may mean that storms may become more numerous (though evidence for this is lacking in the historical record), larger, more persistent, or may deliver more intense rainfall ([24]).

In the absence of a robust alternative, we extrapolate from observed linear trends in maximum annual windspeed and minimum annual pressure twenty-five years into the future (to 2050). Our justification is this: the subtropical Atlantic SST has been increasing at a rate of about 0.4°C per decade since 1993 ([56]). Assuming current mean SST of 25 °C in the subtropical Atlantic, we would expect to be approaching the temperature range associated with "saturation" of impacts of SST-driven strengthening of TCs around 2050 ([55]). It is in this near-term window, where evidence suggests that trends may hold, that we project the annual maximum storm intersecting with HMP infrastructure to increase to a Category 5 storm by 2050.

At existing levels we see an exponential increases in f_s' with increasing TC strength, any continuation of the trend towards increasing strength in the annual maximum TC may markedly increase HMP failure frequency. Increasing trends in TC-related HMP failure across the United States suggest that these increases are associated with both increased vulnerability of HMP infrastructure to TC impacts (indicated by linear trends in v_k and some weak trends in f_o, particularly in Texas, Figure 1b), and increasing intensity of TCs intersecting with HMP infrastructure (indicated by linear trends in TCI, Figure 2a,b). There are multiple potential pipeline-side drivers of increase in both f_o and f_s' over time that are independent of increasing TC intensity, most notably increasing age of pipeline infrastructure and expanding networks (meaning thatboth baseline and TC associated pipeline failures are more likely simply because there is more pipeline to fail). Reports of HMP failures due to all causes have increased markedly in the last fifty years (Figure S1), indicating the growing scope and vulnerability of this essential infrastructure system. Most pipelines in operation today have surpassed 45 years of service, a threshold associated with greater risk of failure ([57]).

These findings underscore the vulnerability of pipeline infrastructure to tropical cyclones (TCs) in general, and major hurricanes in particular. Although natural force damage accounts for only 4.3% of total failures in the PHMSA dataset, we identified that 32.5% of failures in US regions impacted by TC storm tracks occur within 60 days of a TC intersection (Figure S2), and we see that more frequent failures 60 days after a TC intersection are significantly and positively related to TCI, after detrending for non-storm associated failure rates. This provides new data to back previous claims in the literature of under-reporting of TC-related HMP failures ([15]). TC intensity is a statistically significant predictor of both the likelihood and frequency of HMP failures during a storm, with failure frequency increasing exponentially with increasing TCI. This indicates potentially significant exposure to pipeline infrastructure under major hurricanes in particular, and suggests that an increase in intensity of the annual maximum storm is potentially a more impaction variable with regards to predicting future frequency of pipeline failure then an increase in the total number of storms ([24]). Historical data indicates that the annual maximum hurricane intersecting with hazardous material pipeline has increased from a Category 3 storm in 1970 to a Category 4 storm in 2010. Projecting this trend implies that a Category 5 hurricane can be expected to intersect with HMP infrastructure approximately annually by 2050, with strong implications for future HMP failure frequency across the eastern United States. Our results are consistent with current consensus that major hurricanes (category 3 or greater) has increased in observational records in the past fifty years ([24, 46, 58, 59]).

Though limited by the nature of HMP incident reporting data and well-resolved numerical prediction so future Atlantic TC dynamics, these findings strongly supports conclusions from previous research suggesting that TC-associated impacts to HMP infrastructure are under-reported in regulatory record keeping as well as in the scientific literature (e.g.[14]), and stress the need for tailored risk assessments that incorporate complex contributions of natural hazards forcings, including TC forcings, to HMP failure occurrence in incident reports. Given the costs of HMP failures in terms of health, environment, and economic damages, identifying HMP failures associated with TCs are critical to administration of appropriate relief during national emergencies, as well as to improving the accuracy of our accounting of financial damages associated with TC events. If collected, such data could lend insight to improved preparedness measures and targeted mitigation strategies that are essential for safeguarding critical infrastructure against the increasing risks posed by expanding, aging pipeline networks intersecting with intensifying TCs under climate change.

Methods

Data Preparation

This analysis aims to identify TC-associated pipeline failures in the PHMSA database [5]. Prior to 2002, "natural force damages" was not a causal category on incident forms, and post-2002, there is suggested negative reporting bias to this causal category (Text S1, Figure S1, [14]). All data and code comprising this analysis are available online (see SI, [60]). We examine intersections between PHMSA Failure Data (HMP failures) and 6-hourly points in the NOAA HURDAT2 Dataset (TC points, [61]). We merge the datasets by identifying records where HMP failure coordinates fall within the tropical cyclone force diameter (calculated from 34 kt wind radii maximum extent) or, prior to 2004 when the force diameter is unavailable, within a 300 mile (the approximate average tropical cyclone force diameter in the HURDAT 2 database). Additionally, the failures must occur within 60 days of the TC point intersection, where we observe a local inflection in the histogram of latency between HMP failures and TC intesection (Text S1, Figure S2). Before merging, all HMP failures and TC points that fall outside the North American TC storm track region are discarded. If HMP failures do not intersect with any TC points, they are associated with a year specific no-storm identifier. Likewise, TC points that do not intersect with HMP failure points are retained as records in the merged HMP x TC database with no affiliated HMP failure points (Text S1). To account for regional variations in hazardous material pipeline (HMP) failure rates due to factors unrelated to tropical cyclones (e.g., local pipeline construction practices, network length and density, network age, ambient geophysical conditions, and use characteristics), we applied k-means clustering to the latitude and longitude of all records in the merged HMP x TC database to define six spatial sub-regions, each one approximately 300 miles in diameter (Text S1, Figure 1a, [62]).

The merged TC by HMP dataset, which contains records of TCs with no associated HMP failure points, TCs associated with individual HMP failure points, and HMP failure points unassociated with storms, is then aggregated by summing on storm name and region, providing the frequency of HMP failures per TC and per spatial subregion ($f_s^{(i,j,y)}$ or f_s):

$$f_s^{(i,j,y)} = \sum_{\mathrm{x}}\sum_{\mathrm{j'}}\sum_{k'}\eta^{(x,i,j',k')}\delta_{j,j'} \tag{1}$$

Where x is the index for a record in the merged HMP x TC databse; i is the TC intersecting x (with $i* = 0$ reserved for no storm intersection, see Eq 2); *j'* is the spatial subregion of x (defined by k-means cluster), and *k'* is the year of x.

We assume that f_s will include some failures that would have occurred regardless of TC intersection. To adjust for this effect, we define the "background failure frequency" for each location $f_o^{(j,y)}$ as the average 60 day failure frequency unassociated with TC intersections, and allow it to vary over time (as several key drivers of pipeline failure vulnerability are increasing over time, (e.g., increasing pipe age, increasing pipe length). The "background failure frequency" (f_o) is defined as the 5-year 60-day average failure frequency when $i = 0$ (no storm intersection) for each sub-region ($j = 1, \ldots, 6$) for each approximately five-year period ($Y = 1, \ldots, 9$) between 1972 and 2022:

$$f_o^{(j,y)} = \frac{60}{N(Y_y)} \sum_{\text{x}} \sum_{\text{j'}} \sum_{k' \in Y_y} \eta^{(x,i^*,j',k')} \delta_{j,j'} \tag{2}$$

Here Y_y is the set of years in the y^{th} 5-year period between 1972 and 2022 (bounded by years 1985, 1990, 1995, 2000, 2005, 2010, 2015, and 2022), i^* specifically refers to no TC affiliation, and $N(Y_y)$ is the total number of days in Y_y. The storm-related failure frequency ($f_s'^{(i,j,y)}$ or f_s') is then defined as the and subtracted from each storm-associated frequency ($f_s^{(i,j,y)}$), resulting in the storm-related failure frequency ($f_s'^{(i,j,y)}$, Eq. 3):

$$f_s'^{(i,j,y)} = \max\left(f_s^{(i,j,y)} - f_o^{(j,y)}, 0\right) \tag{3}$$

Model Fitting

Due to the multilevel nature of the data and the presence of zero values in f_s' (Eq. 2 and 3), we employed strategically nested mixed-effects logistic (Text S2, S7) and mixed-effects Poisson regressions (Text S3 and S8; Figure S7; Table S1). These models used TC intensity (TCI, derived as the first principal component of regional maximum TC wind speed and regional minimum TC pressure) as the main predictor variable (Text S1). The mixed-effects Poisson regression allows us to predict f_s', a count variable, as a function of TCI, a continuous variable (Text S3 and S7, Figures S8; Table S2):

$$\log(\lambda_{ijk}) = \beta_0 + \beta_1 TCI_{ijk} + u_j + v_k + \gamma_j TCI_{ijk} + \epsilon_{ijk} \tag{4}$$

Here, λ_{ijk} is the expected storm HMP failure frequency for the i-th storm in the j-th region and k-th year; TCI_{ijk} is TC intensity for the i-th storm in the j-th region and k-th year; and β_0 is the overall log-rate intercept. β_1 is the fixed log-rate coefficient for the predictor TCI_{ijk}; u_j is the random intercept for region j, capturing the residual deviation of the j-th region from the overall intercept; v_k is the random intercept for year k, capturing the residual deviation of the k-th year from the overall intercept; γ_j represents the random log-rate coefficient local to each region j; and ϵ_{ijk} is the residual error term. The "full" model (Eq 4) is compared to a null model with no fixed effects (Eq 5):

$$\log(\lambda_{ijk}) = \beta_0 + u_j + v_k + \epsilon_{ijk} \tag{5}$$

The panel model structure mitigates variance bias associated with omitted variables and non-independence of observations ([60, 63]), and the nested panel model structure (comparing Eq 4 to Eq 5) enables a more detailed examination of how temporal (year) and spatial (region) variability in f_s' is influenced by TCI. The model assumes variance component partitioning between random effects, where $u_j(i) \sim \mathcal{N}(0, \sigma^2_{\mathrm{j}})$, $v_k(i) \sim \mathcal{N}(0, \sigma^2_{\mathrm{k}})$, and $\epsilon_{ijk} \sim \mathcal{N}(0, \sigma^2_{\epsilon})$ (Text S4, S5).

Estimating Trends and Future Predictions

Historical (1970–2022) trends in annual TC minimum sea-level pressure ("pressure") and maximum sustained near-surface wind speed ("windspeed") were quantified using ordinary least squares (OLS) regression. We make a simplified, but necessary, assumption that the linear trends will remain constant until 2050 (see discussion and Text S6 for justification and limitations to this approach), and use these models to estimate the 1970, 2010, and 2050 annual maximum TC windspeed and minimum pressure, both globally and for each region (Figure S6). These values are converted to the 1970, 2010, and 2050 TCI using the principal components model trained on historical TC data. TCI values input into the trained Poisson mixed-effects model (Eq 2) to predict storm-associated failure frequency (f_s') associated with the regional annual maximum TCI for 1970, 2010, and 2020.

Acknowledgments

The historical tropical cyclone data used in this study were obtained from the National Hurricane Center's HURDAT2 dataset (Hurricane Database version 2), which is available from the National Oceanic and Atmospheric Administration (NOAA). We acknowledge the Pipeline and Hazardous Materials Safety Administration (PHMSA) for providing the Failure Database, which is a vital resource for tracking and analyzing pipeline failures. Funding for M. Smith was provided by the Graduate Education for Minorities (GEM) Fellowship Program, https://www.gemfellowship.org.

Author Contributions

M.S.: Conceptualization, Methodology, Formal analysis, Writing—original draft.
E.C.: Conceptualization, Methodology, Formal analysis, Writing—original draft, Writing-revision, Data curation, Software, Validation, Visualization, Supervision, Project administration.

Conflicts of Interest

The authors claim no conflicts of interest.

Data availability statement

All data and processing code are available on GitHub at https://github.com/LizCarter492/TCpipeline .

References

1. Parfomak, P. W. DOT's federal pipeline safety program: Background and issues for congress. *Congressional Research Service* (2023).
2. International Energy Agency. *Key world energy statistics 2016* (OECD, 2016).
3. Sovacool, B. K. The costs of failure: A preliminary assessment of major energy accidents, 1907–2007. *Energy Policy* **36,** 1802–1820 (2008).
4. Mignan, A., Spada, M., Burgherr, P., Wang, Z. & Sornette, D. Dynamics of severe accidents in the oil & gas energy sector derived from the authoritative ENergy-related severe accident database. *PLoS one* **17,** e0263962 (2022).
5. US Department of Transportation Pipeline and Hazardous Materials Safety Administration. *Gas Distribution, Gas Gathering, Gas Transmission, Hazardous Liquids, Liquefied Natural Gas (LNG), and Underground Natural Gas Storage (UNGS) Annual Report Data* 2023.
6. Restrepo, C. E., Simonoff, J. S. & Zimmerman, R. Causes, cost consequences, and risk implications of accidents in US hazardous liquid pipeline infrastructure. *Int. J. Crit. Infrastruct. Prot.* **2,** 38–50 (2009).
7. Belvederesi, C., Thompson, M. S. & Komers, P. E. Statistical analysis of environmental consequences of hazardous liquid pipeline accidents. *Heliyon* **4,** e00901 (2018).
8. Maxwell, K., Kiessling, B. & Buckley, J. How clean is clean: a review of the social science of environmental cleanups. *Environ. Res. Lett.* **13,** 083002 (2018).
9. *U.S. Government Publishing Office. Title 49 - Transportation. Parts 191 - 195* 1970.
10. Armstrong Jr, M. F. The Natural Gas Pipeline Safety Act of 1968. *Nat. Resources Law.* **2,** 142 (1969).
11. Zakikhani, K., Nasiri, F. & Zayed, T. A review of failure prediction models for oil and gas pipelines. *Journal of Pipeline Systems Engineering and Practice* **11,** 03119001 (2020).
12. Ricci, F., Casson Moreno, V. & Cozzani, V. A comprehensive analysis of the occurrence of Natech events in the process industry. *Process Saf. Environ. Prot.* **147,** 703–713 (2021).
13. Lam, C. & Zhou, W. Statistical analyses of incidents on onshore gas transmission pipelines based on PHMSA database. *Int. J. Pressure Vessels Piping* **145,** 29–40 (2016).
14. Girgin, S. & Krausmann, E. Analysis of pipeline accidents induced by natural hazards. *European Union: Brussels, Belgium* (2014).

15. Girgin, S. & Krausmann, E. Lessons learned from oil pipeline natech accidents and recommendations for natech scenario development. *Institute for the Protection and Security of the Citizen. Elisabeth Krausmann, Address: Joint Research Centre, Via E. Fermi* **2749,** 21027 (2015).

16. Abraham, J. P. *et al.* A review of global ocean temperature observations: Implications for ocean heat content estimates and climate change: REVIEW OF OCEAN OBSERVATIONS. *Rev. Geophys.* **51,** 450–483 (2013).

17. Keil, P. *et al.* Multiple drivers of the North Atlantic warming hole. *Nature Climate Change* **10,** 667–671 (2020).

18. Cheng, L. *et al.* New record ocean temperatures and related climate indicators in 2023. *Advances in Atmospheric Sciences* **41,** 1068–1082 (2024).

19. Vecchi, G., Landsea, C., Zhang, W., Villarini, G. & Knutson, T. Changes in Atlantic major hurricane frequency since the late-19th century. *Nat. Commun.* **12,** 4054 (2021).

20. Guzman, O. & Jiang, H. Global increase in tropical cyclone rain rate. *Nat. Commun.* **12,** 5344 (2021).

21. Reed, K. A., Wehner, M. F. & Zarzycki, C. M. Author Correction: Attribution of 2020 hurricane season extreme rainfall to human-induced climate change. *Nat. Commun.* **13,** 2589 (2022).

22. Pielke Jr, R. A. *et al.* Normalized Hurricane Damage in the United States. *Nat. Hazards Rev.* (2005).

23. Mallard, M. S., Lackmann, G. M., Aiyyer, A. & Hill, K. Atlantic hurricanes and Climate Change. Part I: Experimental design and isolation of thermodynamic effects. *J. Clim.* **26,** 4876–4893 (2013).

24. Camargo, S. J. *et al.* An update on the influence of natural climate variability and anthropogenic climate change on tropical cyclones. *Tropical Cyclone Research and Review* **12,** 216–239 (2023).

25. Nair, G. S., Dash, S. & Mondal, G. Review of Pipeline Performance during Earthquakes since 1906. *J. Perform. Constr. Facil.* **32,** 04018083 (2018).

26. Murphy, J. F. & Conner, J. Beware of the black swan: The limitations of risk analysis for predicting the extreme impact of rare process safety incidents. *Process Saf. Prog.* **31,** 330–333 (2012).

27. Czajkowski, J., Simmons, K. & Sutter, D. An analysis of coastal and inland fatalities in landfalling US hurricanes. *Nat. Hazards (Dordr.)* **59,** 1513–1531 (2011).

28. Qin, R., Khakzad, N. & Zhu, J. An overview of the impact of Hurricane Harvey on chemical and process facilities in Texas. *Int. J. Disaster Risk Reduct.* **45,** 101453 (2020).

29. Burow, D., Ellis, K. & Tran, L. Simultaneous and collocated tornado and flash flood warnings associated with tropical cyclones in the contiguous United States. *Int. J. Climatol.* **41,** 4253–4264 (2021).

30. Cruz, A. M., Steinberg, L. J. & Vetere-Arellano, A. L. Emerging issues for natech disaster risk management in Europe. *Journal of Risk Research* **9,** 483–501 (2006).

31. Kishné, A. S., Morgan, C. & Miller, W. Vertisol crack extent associated with gilgai and soil moisture in the Texas Gulf Coast Prairie. *Soil Science Society of America Journal* **73,** 1221–1230 (2009).

32. Tamizdoust, K., Farzi Sizkow, S., AbdelHamid, Y., Helal, A. & Bryant, J. T. in *Forensic Engineering* 714–724 (ASCE, 2024).

33. Li, X. *et al.* Effect of residual and external stress on corrosion behaviour of X80 pipeline steel in sulphate-reducing bacteria environment. *Engineering Failure Analysis* **91,** 275–290 (2018).

34. Wang, H., Yajima, A., Liang, R. Y. & Castaneda, H. A clustering approach for assessing external corrosion in a buried pipeline based on hidden Markov random field model. *Structural Safety* **56,** 18–29 (2015).

35. Girgin, S. & Krausmann, E. Historical analysis of U.S. onshore hazardous liquid pipeline accidents triggered by natural hazards. *J. Loss Prev. Process Ind.* **40,** 578–590 (2016).

36. Sengul, H., Santella, N., Steinberg, L. J. & Cruz, A. M. Analysis of hazardous material releases due to natural hazards in the United States. *Disasters* **36,** 723–743 (2012).

37. Edwards, R. Tropical cyclone tornadoes: A review of knowledge in research and prediction. *Electron. J. Sev. Storms Meteorol.* **7,** 1–61 (2021).

38. Booth, J. F., Narinesingh, V., Towey, K. L. & Jeyaratnam, J. Storm surge, blocking, and cyclones: A compound hazards analysis for the Northeast United States. *J. Appl. Meteorol. Climatol.* **60,** 1531–1544 (2021).

39. Lai, Y., Li, J., Gu, X., Liu, C. & Chen, Y. D. Global compound floods from precipitation and storm surge: Hazards and the roles of cyclones. *J. Clim.* **34,** 1–55 (2021).

40. Olive, W. W. *et al. Swelling clays map of the conterminous United States* 1989.

41. Clayton, C. R. I., Xu, M., Whiter, J. T., Ham, A. & Rust, M. Stresses in cast-iron pipes due to seasonal shrink-swell of clay soils. *Proceedings of the Institution of Civil Engineers - Water Management* **163,** 157–162 (2010).

42. Shen, W., Tuleya, R. E. & Ginis, I. A sensitivity study of the thermodynamic environment on GFDL model hurricane intensity: Implications for global warming. *Journal of Climate* **13,** 109–121 (2000).

43. EPA. *Inter- and intra-state pipelines for natural gas in the United States and its territories* `https://www.arcgis.com/home/item.html?id=461c53a9c05f4fc19b1017c96e8a03c0`. Accessed: 2025-05-08. 2020.

44. Weaver, M. M. & Garner, A. J. Varying genesis and landfall locations for North Atlantic tropical cyclones in a warmer climate. *Scientific Reports* **13,** 5482 (2023).

45. Holland, G. & Bruyère, C. L. Recent intense hurricane response to global climate change. *Clim. Dyn.* **42,** 617–627 (2014).

46. Kossin, J. P., Knapp, K. R., Olander, T. L. & Velden, C. S. Global increase in major tropical cyclone exceedance probability over the past four decades. *Proc. Natl. Acad. Sci. U. S. A.* **117,** 11975–11980 (2020).

47. Elsner, J. B. Evidence in support of the climate change–Atlantic hurricane hypothesis. *Geophys. Res. Lett.* **33** (2006).

48. Gilford, D. M., Giguere, J. & Pershing, A. J. Human-caused ocean warming has intensified recent hurricanes. *Environ. Res.: Climate* **3,** 045019 (2024).

49. Cione, J. J. & Uhlhorn, E. W. Sea surface temperature variability in hurricanes: Implications with respect to intensity change. *Monthly Weather Review* **131,** 1783–1796 (2003).

50. Cane, M. A. *et al.* Twentieth-century sea surface temperature trends. *science* **275,** 957–960 (1997).

51. Kaplan, A., Kushnir, Y., Cane, M. A. & Blumenthal, M. B. Reduced space optimal analysis for historical data sets: 136 years of Atlantic sea surface temperatures. *Journal of Geophysical Research: Oceans* **102,** 27835–27860 (1997).

52. Karnauskas, K. B., Zhang, L. & Amaya, D. J. The atmospheric response to North Atlantic SST trends, 1870–2019. *Geophysical Research Letters* **48,** e2020GL090677 (2021).

53. Yang, X. & Huang, P. Improvements in the relationship between tropical precipitation and sea surface temperature from CMIP5 to CMIP6. *Climate Dynamics* **60,** 3319–3337 (2023).

54. Sung, H. M. *et al.* Future changes in the global and regional sea level rise and sea surface temperature based on CMIP6 models. *Atmosphere* **12,** 90 (2021).

55. Tonkin, H., Holland, G. J., Holbrook, N. & Henderson-Sellers, A. An evaluation of thermodynamic estimates of climatological maximum potential tropical cyclone intensity. *Monthly weather review* **128,** 746–762 (2000).

56. ECMWF. *Sea surface temperature* 2023.

57. Awuku, B., Huang, Y. & Yodo, N. Predicting natural gas pipeline failures caused by natural forces: An artificial intelligence classification approach. *Appl. Sci. (Basel)* **13,** 4322 (2023).

58. Emanuel, K. Evidence that hurricanes are getting stronger. *Proceedings of the National Academy of Sciences* **117,** 13194–13195 (2020).

59. Elsner, J. B. Continued increases in the intensity of strong tropical cyclones. *Bulletin of the American Meteorological Society* **101,** E1301–E1303 (2020).

60. Carter, E., Hultquist, C. & Wen, T. GRRIEn analysis: A data science cheat sheet for Earth scientists learning from global Earth observations. *Artificial Intelligence for the Earth Systems* **2,** 1–49 (2023).

61. NHC. *Atlantic hurricane database (HURDAT2) 1851-2023* 2023.

62. Pedregosa, F. *et al.* Scikit-learn: Machine Learning in Python. *J. Mach. Learn. Res.* **abs/1201.0490,** 2825–2830 (2011).

63. F. Dormann, C. *et al.* Methods to account for spatial autocorrelation in the analysis of species distributional data: a review. *Ecography (Cop.)* **30,** 609–628 (2007).

64. Holland, G. A revised hurricane pressure–wind model. *Monthly Weather Review* **136,** 3432–3445 (2008).

65. Knutson, T. *et al.* Tropical cyclones and climate change assessment: Part I: Detection and attribution. *Bull. Am. Meteorol. Soc.* **100,** 1987–2007 (2019).

66. Kossin, J. P. Hurricane intensification along United States coast suppressed during active hurricane periods. *Nature* **541,** 390–393 (2017).

67. Michanowicz, D. R. *et al.* A national assessment of underground natural gas storage: identifying wells with designs likely vulnerable to a single-point-of-failure. *Environ. Res. Lett.* **12,** 064004 (2017).

68. Qin, G., Zhang, P., Hou, X., Wu, S. & Wang, Y. Risk assessment for oil leakage under the common threat of multiple natural hazards. *Environ. Sci. Pollut. Res. Int.* **27,** 16507–16520 (2020).

69. De Luca, P., Hillier, J. K., Wilby, R. L., Quinn, N. W. & Harrigan, S. Extreme multi-basin flooding linked with extra-tropical cyclones. *Environ. Res. Lett.* **12,** 114009 (2017).

70. Czajkowski, J., Villarini, G., Montgomery, M., Michel-Kerjan, E. & Goska, R. Assessing current and future freshwater flood risk from north Atlantic tropical cyclones via insurance claims. *Sci. Rep.* **7,** 41609 (2017).

71. Knutson, T. *et al.* Tropical cyclones and climate change assessment: Part I: Detection and attribution. *Bull. Am. Meteorol. Soc.* **100,** 1987–2007 (2019).

72. Cruz, A. M. & Krausmann, E. Vulnerability of the oil and gas sector to climate change and extreme weather events. *Climatic change* **121,** 41–53 (2013).

73. Elsner, J. B. Hurricanes and climate change. *Bull. Am. Meteorol. Soc.* **89,** 677–679 (2008).